Applied Clay Science 205 (2021) 106065

Contents lists available at ScienceDirect

Applied Clay Science

journal homepage: www.elsevier.com/locate/clay

Research Paper

Clay coatings on sands in the western Qaidam Basin, Tibetan Plateau, China: Implications for the Martian clay detection

Yonglei Zhang [a,b], Qi Tao [a,c,*], Sridhar Komarneni [d], Jiacheng Liu [e], Yang Zhou [a,b], Fan Yang [f], Baifa Zhang [a,b]

[a] CAS Key Laboratory of Mineralogy and Metallogeny & Guangdong Provincial Key Laboratory of Mineral Physics and Materials, Guangzhou Institute of Geochemistry, Chinese Academy of Sciences, Guangzhou 510640, PR China
[b] University of Chinese Academy of Sciences, Beijing 100049, PR China
[c] CAS Center for Excellence in Deep Earth Science, Guangzhou 510640, PR China
[d] Department of Ecosystem Science and Management and Materials Research Institute, 204 Energy and the Environment Laboratory, The Pennsylvania State University, University Park, PA 16802, USA
[e] Department of Earth Sciences, The University of Hong Kong, Hong Kong, PR China
[f] Key Laboratory of Mineral Resources in Western China (Gansu Province), School of Earth Sciences, Lanzhou University, Lanzhou 730000, PR China

ARTICLE INFO

Keywords:
Clay minerals
Coatings
Martian clay
Martian analog
Qaidam Basin

ABSTRACT

The widespread clay minerals on Mars have been detected using orbital data using near-infrared spectroscopy, which is limited by its shallow detection depth, low recognition precision and resolution, and can only be qualitative etc. Terrestrial analogues on the Earth provide valuable guidance to further understand the distribution and occurrence of clay minerals on Mars. In this study, seven detrital samples with clay minerals as coatings (Abbreviated as "clay coatings") were collected from four sites in the western Qaidam Basin, a Martian analogue terrain. We identify the mineralogy of the surface coatings to be illite and chlorite, as confirmed by a combination techniques of X-Ray Diffraction (XRD), Scanning Electron Microscope (SEM), Electron Probe X-ray Microanalysis (EPMA) and Near-infrared spectroscopy (NIR). The NIR results suggested that merely small amounts of clay minerals (~0.5 mg/cm^2 and about several micrometers in thickness) masking the surface of sands could lead to well-distinguished characteristic NIR absorption, and their band depth could reach those measured from Martian soil analogues with ~5 $_{wt}$% to 25 $_{wt}$% clay minerals at 2.20–2.40 μm. The results of the synthesized samples as coating analogues with clay minerals coated on the surface of quartz grains showed a consistent trend as that of the field samples on the Earth. The further mineralogical analysis indicated that the origin of clay minerals in the coatings of Qaidam Basin is of Aeolian source. Environmental similarities between western Qaidam Basin and Martian surface suggested that various rock coatings potentially exist on Mars and they could affect the mineral detection and the accuracy of mineral identification by remote sensing.

1. Introduction

Near-infrared reflectance spectroscopy (NIR), with a detection wavelength region of 800–2500 nm, is one of most regularly utilized measurement for the determination of mineralogical composition on Martian surface both from orbit and in situ with Mars rovers. Dozens of minerals on the Mars surface, including phyllosilicates, hydrated silica, sulfates, carbonates, oxides and hydroxides, had been identified by using reflectance, emission and elemental spectrometers in the last several years (Bishop et al., 2008; Carter et al., 2010; Ehlmann et al., 2013; Gaudin et al., 2018).

Clay minerals arouse particular interests, because as hydrous minerals, they recorded an interaction with liquid water (Bibring et al., 2006; Cuadros et al., 2013), and the geological evolution of the Martian surface (Ehlmann et al., 2009; Carter et al., 2010; Cino et al., 2017). Therefore, to understand the abundance, distribution and occurrence of clay minerals on Mars is one of the prerequisites to reveal the evolution of climate, environment, geomorphology, lithology and ancient oceans during the early Mars history (Ehlmann et al., 2013). Abundant clay minerals had been identified globally using data acquired from orbital spectrometers, including smectites (e.g, saponite, nontronite and montmorillonite), chlorite, kaolinite and illite (Ehlmann and Edwards,

* Corresponding author at: Guangzhou Institute of Geochemistry, Chinese Academy of Sciences, No. 511 Kehua Street, Guangzhou 510640, China.
E-mail address: taoqi@gig.ac.cn (Q. Tao).

https://doi.org/10.1016/j.clay.2021.106065
Received 21 November 2020; Received in revised form 10 March 2021; Accepted 12 March 2021
Available online 21 March 2021

2014; Montagnac et al., 2020). However, their origins and formation mechanisms have not yet been well resolved, due to the absence of more detailed in-situ measurements and/or the resolution limitations from instruments and precise geological context during the exploration of Mars (Michalski and Fergason, 2009; Ehlmann et al., 2013; Bridges et al., 2015).

Rock coating is a term that has not yet been formally approved, which refers to class of secondary materials formed as a thin layer on the rock formed under different genesis conditions (Dorn, 1998; Minitti et al., 2007; Duteil et al., 2020). They are mainly produced at arid zones during hydrological or pedological processes. Ubiquitous rock coatings with various compositions were confirmed on the surface of the Earth as well as the Mars by chemical and spectral measurements (Christensen, 2004; Chemtob et al., 2010; Marnocha, 2017), which included dust coatings, hematite coatings, desert varnishes, salt-cemented coatings and silica glazes (Seelos et al., 2010; Marnocha and Dixon, 2013). As for the Mars, the compositions of coatings on Mars could consist of fine-grained basalt, iron oxide, silica, clay minerals etc. (Minitti et al., 2007; Ehlmann et al., 2009; Meslin, 2013; Lefebvre et al., 2016). On one hand, rock coatings had already been proved to record geologically valuable information, such as relative ages of flow surfaces, palaeoclimate, wind abrasion rate and the physical and chemical interactions between the substrate and the surrounding environment (Dorn, 1998; Kraft et al., 2003; Clark et al., 2016; Schindler and Dorn, 2017). On the other hand, however, the presence of such a coating would cause the weakening, deviation and distortion of the spectral signature as observed both in remote sensing and in situ detections (Christensen, 2004; Minitti et al., 2007; Farrand et al., 2016). This may greatly increase the chance of errors during spectral analysis, such as thermal infrared analysis (TIR), and visible and near infrared reflectance analyses (VNIR), and therefore distort understanding of the exact substrate lithology (Seelos et al., 2010).

The western Qaidam Basin, located in Tibetan Plateau of China, has been widely masked by detrital sands with various types of coatings, in which halite coatings, dust coatings, clay coatings and desert varnish (often called “rock varnish”) have been mentioned (Schubel and Lowenstein, 1997; Xie et al., 2018; Chen et al., 2019). The detrital sands are composed of gravels or single minerals with the size of a few to dozens of millimeters dominantly. It was considered a unique analogue site to the Mars, because it had been developed geomorphic structures (i.e. playas, driest deserts, aeolian dunes, yardangs, polygons and gullies) and mineral compositions (i.e. evaporite mineral assemblages) similar to those discovered on the Martian surface by the extremely arid and cold climate (Xiao et al., 2017; Dang et al., 2018). This study focuses on clay minerals coatings (Abbreviated as “clay coatings” hereinafter) that were coated on detrital sands of Tibetan Plateau of China. The phases, composition and morphology characteristics were analyzed by using a combination of techniques, including Near-infrared spectroscopy (NIR), X-ray diffraction (XRD), Electron Probe X-ray Microanalysis (EPMA) and Scanning Electron Microscopy (SEM). Subsequently, three synthetic samples are developed using four clay mineral standards (e.g., illite, chlorite, kaolinite and montmorillonite) and quartz. We simulate different clay mineral coatings on quartz grains as substrate to disclose the influences of clay coatings with different composition ratios, thickness and occurrence state on the NIR spectral characteristics, which was potentially existing on Mars. The aim of this study is to provide a possible perspective on the distribution and petrological context of clay minerals on Mars.

2. Samples and methods

2.1. Background and samples

2.1.1. Geological setting of the Qaidam Basin

The Qaidam Basin, is a vast intermountain basin (with an area of more than 2×10^5 km^2), surrounded by Altun Mountain, Qilian Mountain and Kunlun Mountain, and located in the northern Tibetan Plateau, China (Fig. 1). It has been subject to an environment with an arid and cold climate since the Pleistocene, causing the formation of wind erosion landforms (Xiao et al., 2017). Many geomorphic structures including playas, driest deserts, aeolian dunes, yardangs, polygons and gullies, and minerals including evaporite mineral assemblages, particularly in western Qaidam Basin, are similar to those discovered on Martian surface (Dang et al., 2018).

Various types of aeolian detrital sediments are ubiquitously distributed on the surface of Qaidam Basin. The upper surface is dominated by quartz, followed by feldspar; and the lower surface is mainly composed of halite, calcite and a minor amount of clay minerals with weak weathering resistance (Dang et al., 2018). The surface sediments were subject to physical weathering and mechanical transportation by wind (Chen and Bowler, 1986; Wu et al., 2012; Yu and Lai, 2012). The origin of sand sediments mainly includes weathered materials from the surrounding mountains and lacustrine sediments after salt lake shrinking (Bao and Dong, 2015).

2.1.2. Samples

Seven detrital sediment samples (Fig. S1) with coatings were collected from four sites in the western Qaidam Basin, which included Site I at 37.91°N, 91.84°E (Marked as IL1, ID2, ID3, and IL4), Site II at 38.01°N, 91.83°E (Marked as IID1), Site III at 38.45°N, 92.15°E (Marked as IIIL1), and Site IV at 38.04°N, 91.43°E (Marked as IVL1) (Fig. 1b), respectively. The samples can be divided into dark- and light-colored samples (Marked as D- and L-, respectively) according to their color (Fig. 2).

The separation of coatings followed the combination of the Stokes sedimentation method (Stokes, 1945), and sedimentation siphon separation method. The light- and dark-colored samples were firstly subject to ultrasonic in a beaker for 20 min. After that, the suspensions of the light-colored samples were transferred to the siphon tubes for a 20-min sedimentation. Subsequently, the suspensions were extracted at a depth of 10 cm in the upper layer. In the case of the dark-colored samples, they were washed first by deionized water, followed by ultrasonic treatment for another 50 min, and then treated and extracted with the same procedures as those used for the light-colored samples. The collected suspensions with a particle size of *ca.* 10.00 μm were centrifuged, concentrated and sedimentated for the further characterizations.

2.2. Analysis methodology

XRD patterns were collected with a Bruker D8 Advance diffractometer (Germany), operating at 40 kV and 40 mA using CuKα radiation. The specimens were investigated from 3° to 70° (2θ) with a scanning speed of 3°/min.

Elements and morphological analysis were performed by JEOL JXA-8100 machine at 20 kV accelerating voltage, 10 nA beam current, 10 μm spot, and 30 s peak counting time, and a HITACHI SU8010 field-emission scanning electron microscope (FESEM, Japan) at an accelerating voltage of 15 kV, respectively. All the above characterizations were performed at Guangzhou Institute of Geochemistry, Chinese Academy of Sciences.

NIR analyses were recorded using an FieldSpec 4 Hi-Res spectrometer (ASD, Analytical Spectral Devices Company) at Beijing Yaowangtianji Sci. & Tech. Ltd. The ASD spectrometer was setup according to the ASD FieldSpec 4 user’s manual. Spectral measurements were carried out in the range from 350 to 2500 nm. The spectral resolutions are 3 nm and 10 nm for the range of 350–1000 nm and 1000–2500 nm, respectively. An accessory light source was employed to measure spectrum without sunlight. During the measurements, the detector was attached to a relatively flat surface of the rock sample to avoid possible influence from fluorescence lighting in the environment. A white reference made of Teflon with the reflectance value of approximately 100% was introduced in the measuring procedure to optimize and

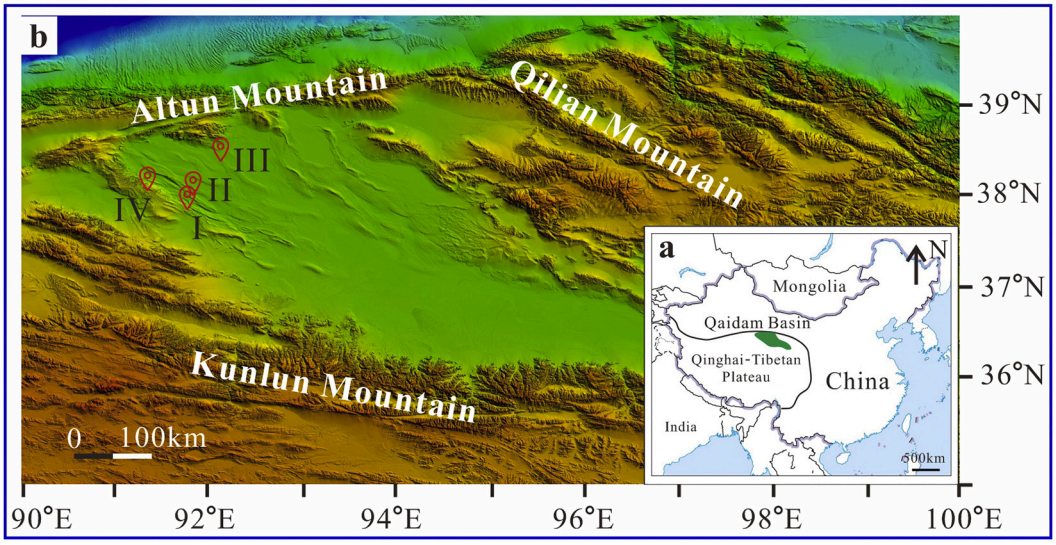

Fig. 1. Geological map of the investigated area in the west Qaidam Basin. (a) The location (green area) of the Qaidam Basin. (b) Digital elevation model map of the Qaidam Basin. I-IV: Sampling sites (Marked with red signs).

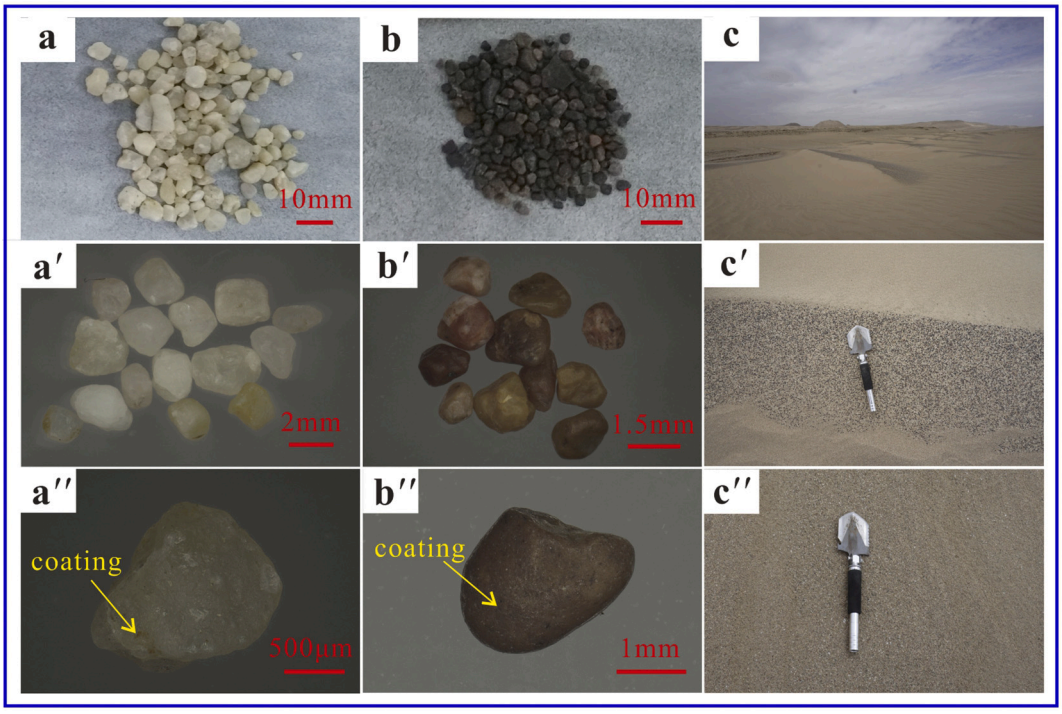

Fig. 2. Sample photographs (a and b) and stereoscopic photographs (a', a", b' and b") of the hand specimens. (Serials a (a - a") and Serials b (b - b") representative the light-and dark-colored samples, respectively); (c, c' and c") Landscape of sampling sites for both samples.

calibrate the instrument. For each sample, five spectra were recorded using the RS^3 software. To facilitate comparison of the combination bands (1.80–2.50 μm), the spectral continuum was removed from 0.35 to 2.50 μm for all spectra using a straight-line continuum across the extreme convex points (Bishop et al., 2008). Spectral band depths of four clay minerals in our Synthesized samples were calculated according to the formulas from Clark and Roush (1984) and Viviano-Beck et al. (2014), Which was detailed in Supplementary material Text S1 and Fig. S2.

2.3. Synthesized samples

Martian soil, formed mainly by physical weathering of the Martian crust, is basaltic in composition (Hamilton and Christensen, 2005; Guan et al., 2020). Two synthesized samples (Synthesized samples A and Synthesized samples B) of four clay mineral samples (illite, chlorite, kaolinite and montmorillonite) coated quartz were designed to disclose the effects of clay coatings with different thickness and mass ratios on the NIR spectral characters. The four clay mineral, including illite (~95%, collected in Hebei Province, China), chlorite (~90%, collected in Liaoning Province, China), kaolinite (~95%, collected in Jiangxi Province) and montmorillonite (~95%, collected in Inner Mongolia,

China), are all natural samples collected from Sample Library of Key Laboratory of Mineralogy and Metallogeny, Guangzhou Institute of Geochemistry, Chinese Academy of Sciences. The clay mineral content was estimated by K value method. Synthesized samples C was designed as an analogue of the Martian soil. The particle sizes of the selected coating analogues (clay minerals) were controlled below 300 mesh (He et al., 2013).

2.3.1. Synthesized samples A: trace amount of clay coatings on the quartz grains

The quartz grains with a size of ~5 mm (close to the mean size of field samples) and four clay minerals were chosen as substrate and coating analogues, respectively (Table 1). The homogeneous suspensions of the four clay minerals were prepared separately by an ultrasonic treatment with a concentration of 40.0 mg/ml. Then, four aliquots of quartz grains (~0.6 g each) were added to the suspensions. The mixtures were mixed with a rotating device for a week. After decanted the residual suspensions, the quartz grains were rinsed with deionized water to remove the clay minerals, which did not adhered to the quartz substrate. Finally, the coating analogues were dried at 60 °C for 24 h and stored for the further measurements.

2.3.2. Synthesized samples B: clay minerals coating on the polished surface of quartz

Four homogeneous clay suspensions (1.0 ml each), with clay concentrations of 1.6, 8.0 and 40.0 mg/ml were titrated on the surface of polished quartz with an area of ~3 cm^2, respectively. After air-drying at room temperature (R.T.) for 24 h, the coatings were further dried at 50 °C for 12 h. Assuming that the clay minerals (with an average density of 2.6 g/cm^3) were uniformly distributed on the polished surface, the thickness of the above coatings could be calculated as *ca.* 2.1, 10.5 and 50.3 μm, respectively.

2.3.3. Synthesized samples C: clay minerals in the Martian soil analogues

To simulate clay minerals mixed with Martian soil (i.e., weathered basalt) (Meslin, 2013), Synthesized samples C was designed by physically mixing basalt grains with different contents of clay minerals (~1 $_{wt}$%, ~5 $_{wt}$%, ~12 $_{wt}$ %, ~25 $_{wt}$%, ~40 $_{wt}$% and ~ 55$_{wt}$%), respectively. The size ratios of the basalt grains were selected according to the Martian soil simulants (<20 mesh: ~15%; 20–100 mesh: ~60%; 100–200 mesh: ~12%; >200 mesh: ~13%) (Guan et al., 2020). The basalt in this study were collected in Shandong Province, China. The detailed compositional information of the soil simulant used were as follow (Table 2):

3. Results

3.1. X-ray diffraction (XRD)

XRD patterns of the seven field samples (powder of detrital sands; black line) show a serial of reflections with d-values at ~0.43, 0.33 and 0.18 nm, corresponding to (100), (101) and (112) crystal faces of quartz, respectively (Fig. 3a). For their respective ultrasonic treated products (suspended solids in suspension with a particle size of *ca.*10.00 μm after centrifugation, concentration and sedimentation; red line), the XRD patterns show that the reflections with d-values at ~1.00 and 0.33 nm were ascribed to (001) and (006) of illite, respectively (Fig. 3b). The d-values of ~1.41, 0.71 and 0.35 nm, correspond to (001), (002) and (004) reflections of chlorite, respectively (Fig. 3b). Before ultrasonic treatment (black line), quartz was the major mineral for all samples (Fig. 3a). After ultrasonic treatment (red line), a small amount of clay minerals (illite and chlorite) appeared, together with the major amount of quartz (Fig. 3b).

Table 1
The compositions of coatings in Synthesized samples A.

Clay minerals	Quartz grains (g)	Total mass (g)	Coatings (g)	Coating Contents ($_{wt}$%)
Ill	0.6214	0.6277	0.0013	0.21
Chl	0.6090	0.6131	0.0031	0.51
Kln	0.6280	0.6385	0.0015	0.23
Mnt	0.6128	0.6286	0.0028	0.45

3.2. Visible and near-infrared reflectance spectroscopy (VNIR)

The VNIR spectral features located between 1.40 and 2.50 μm are usually used to distinguish different clay minerals. The overtones of OH stretching in H_2O ($2\nu H_2O$) and M-OH ($2\nu MOH$, M represents for octahedral cations of clay minerals, such as Al, Mg, Fe^{III} and Fe^{II}) that occur at ~1.40 μm. The asymmetric combination bands of H_2O ($(\nu + \delta)_{as}H_2O$) in interlayers or adsorbed on surfaces and M-OH occur at ~1.90 and 2.20–2.40 μm, respectively (Chemtob et al., 2015). Bands from 2.20 to 2.40 μm vary depending on substitution of cations such as Al, Fe, and Mg in octahedral and tetrahedral sheets of layers.

The light-colored samples (IL1, IL4, IIIL1 and IVL1) show the NIR bands near 2.25 μm and 2.35 μm (Fig. 4), which are attributed to the combination bands of AlFe-OH and Fe(II)-OH of iron-rich clay minerals. While the band at 2.25 μm is weak in the present samples. The intensity of the above bands for the dark-colored samples (ID2, ID3 and IID1), is weaker than those for the light-colored ones, which may have been caused by the lower albedo. Combined with the band features near 2.25 μm and 2.35 μm, the clay minerals in the sand coatings can be ascribed to ferrous iron-rich chlorite.

In both types of samples, the strong absorption near 2.20 μm were probably assigned to the combination bands of Al-OH. Opaline silica can also exhibit a wider band centered at 2.21 μm due to Si-OH bonds (Milliken et al., 2008). Although opaline silica as the major phase was excluded, because of the absent of the broad hump in the region of 20–40° (2θ), which is the characteristic XRD reflection of the amorphous silica. They can be still possibly formed by reprecipitation of amorpous silica on the sands. The existence of illite was confirmed on the coating of the sands by showing the characteristic reflections with d values of ~1.00 and 0.33 nm (Fig. 3). Based on the above discussions, bands near 2.20 μm could be ascribed to the combination bands of Al-OH in illite and Si-OH of opaline silica on the surface coating of sands. The bands near 1.41 μm and 1.92 μm were attributed to overtones and combinations of water in interlayers or adsorbed on surfaces and M-OH in illite and chlorite, respectively.

3.3. Electron microprobe

EPMA results indicated that the main composition of the seven samples was SiO_2 (Fig. S3; Table 3). The elemental linear scans results indicated that, generally, the contents of Al, Fe and Mn in the surface coatings were significantly higher than those in the inner substrates, respectively. Meanwhile, the content of Fe and Mn in the dark- colored samples (e.g., ID2, ID3 and IID1) was higher than those in the light-colored ones (e.g., IL1, IL4, IIIL1 and IVL1). Furthermore, no Mn was detected in the light-colored samples. It was deduced from these results that Fe, Mn and Al were preferentially accumulated on the outer surface of the samples during weathering, and Fe or Mn oxides are the main chemicals that caused the color of the samples to darken.

3.4. Scanning electron microscopy

Detrital materials with foliated morphology had been observed by SEM to mask the surface of sands for all the raw samples (Figs. 5a, d-f). After ultrasonic treatment, the detrital materials were removed (Figs. 5b and c), indicative of an occurrence state of physical attachments in the form of dust coating. The micro pits and hillocks with different shapes were possibly caused by corrosion or impact, and precipitation of the

Table 2
The compositional information of the Martian soil simulant.

Soil simulants containing illite (Ill + B)			Soil simulants containing chlorite (Chl + B)			Soil simulants containing kaolinite (Kln + B)			Soil simulants containing montmorillonite (Mnt + B)		
B (g)	Ill (g)	Ill content ($_{wt}$%)	B (g)	Chl (g)	Chl content ($_{wt}$%)	B (g)	Kln (g)	Kln content ($_{wt}$%)	B (g)	Mnt (g)	Mnt content ($_{wt}$%)
0.5833	0.0068	1	0.5957	0.0060	1	0.5891	0.0071	1	0.5837	0.0080	1
0.5743	0.0416	6	0.5629	0.0317	5	0.5938	0.0339	5	0.5628	0.0325	5
0.5452	0.0722	12	0.5228	0.0774	13	0.5178	0.0739	12	0.5228	0.0801	13
0.3753	0.1228	25	0.3718	0.1215	25	0.3701	0.1258	25	0.3329	0.1225	27
0.2383	0.1559	40	0.2449	0.1507	38	0.2476	0.1604	39	0.2374	0.1613	40
0.0901	0.1090	55	0.0906	0.1160	56	0.1018	0.1180	54	0.0932	0.1173	56

Note: B represents basalt grains with the size ratios of Martian soil simulants (<20 mesh: 15%; 20–100 mesh: 60%; 100–200 mesh: 12%; >200 mesh: 13%) (Guan et al., 2020). Ill, illite; Chl, chlorite; Kln, kaolinite; Mnt, montmorillonite.

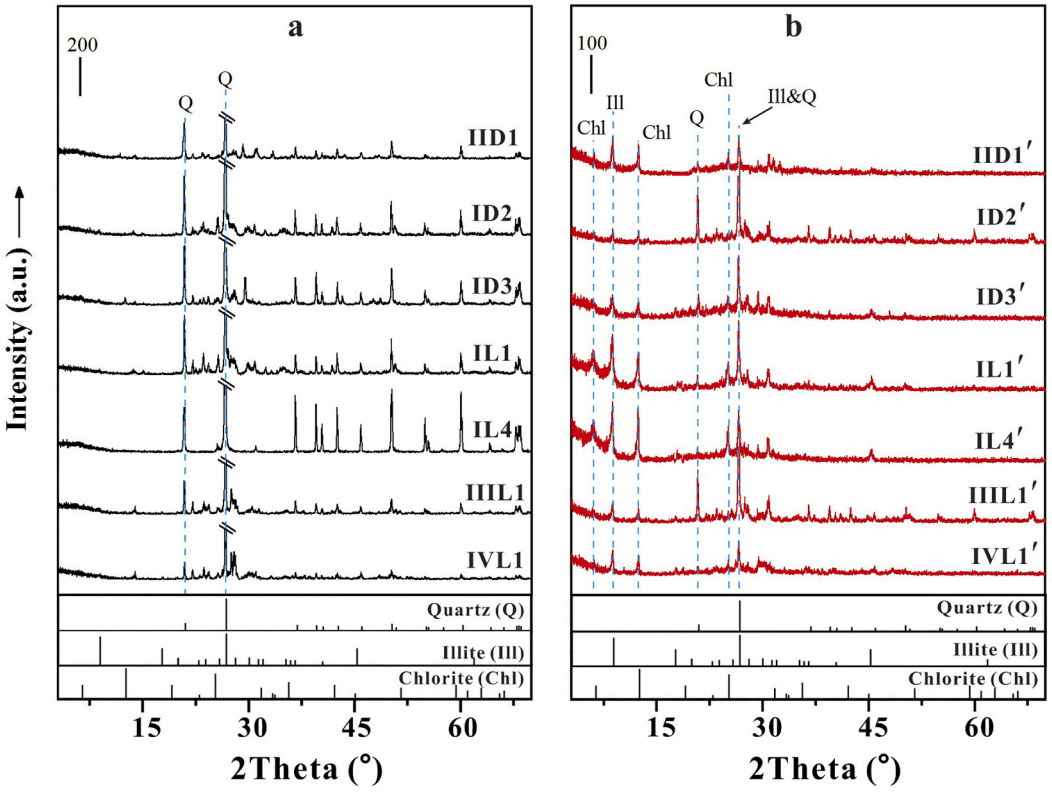

Fig. 3. The XRD patterns of the seven field samples (detrital sands; black line) and their respective ultrasonic treated products (suspended solids in suspension with a particle size of *ca.*10.00 μm after centrifugation, concentration and sedimentation; red line).

products on the surface, respectively (Figs. 5b and c). The sands usually showed an excellent roundness due to weathering, dissolution and reprecipitation of amorphous silica.

Back scattered electron (BSE) images of the slices of dark-colored sand samples (ID2, ID3 and IID1) showed that the outer coatings were distinctly different with the inner substrates in morphology (Figs. 6a-d). The thickness of coatings ranged from several micrometers to more than ten micrometers. For light-colored samples (IL1, IL4, IIIL1 and IVL1), however, the coatings had no obvious thickness (Figs. 6e-h).

3.5. Synthesized samples results

For the samples with the minor clay coating on the quartz grains, although the mass concentrations of the masked coatings are very low (<0.51 $_{wt}$%), the phases of the coated minerals can still be distinguished by NIR (Table 1, Fig. 7a). For chlorite coating (0.51 $_{wt}$%), the two characteristic bands of chlorite were distinctively shown at ca. 2.24 μm and 2.32 μm, corresponding to AlFe-OH and Fe-OH combinations, respectively (Fig. 7a). The band near 2.20 μm of kaolinite coating (0.23 $_{wt}$%) was also clear but with the lowest intensity, corresponding to Al_2-OH combination ($\nu_4 + \delta$). However, the other characteristic band at ca. 2.16 μm was missing that corresponded to another Al_2-OH combination ($\nu_1 + \delta$). The intensity of Al-OH related combination bands was the strongest among the four clay coatings, which was located at 2.21 and 2.20 μm as for montmorillonite (0.45 $_{wt}$%) and illite (0.21 $_{wt}$%), respectively.

In order to reduce the error caused by the thickness and uniformity difference of coverage, polished quartz with flat surface and certain area was adopted as substrates, covered by a serial of clay mineral suspensions with specific concentrations (Synthesized samples B). NIR results showed that the intensity of combination bands between 2.10 and 2.40 μm decreased with the decrease of clay mineral concentrations on the polished surface of quartz (Fig. 7b). For the samples with the coatings masses as 8.0 mg (~2.7 mg/cm^2) and 40.0 mg (~13.3 mg/cm^2) on the polished surface, the M-OH combination bands of four clay minerals could be clearly identified no matter what kind of clay mineral it was.

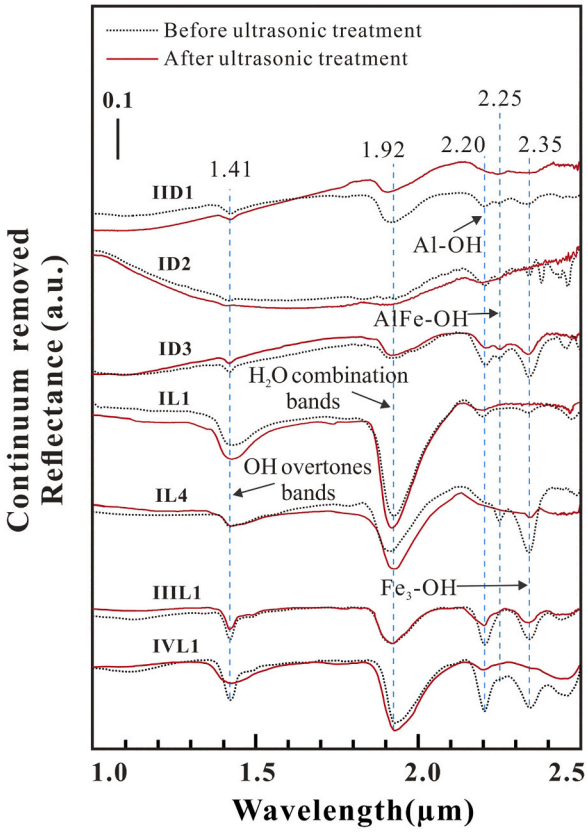

Fig. 4. NIR Spectra of the field samples before (dotted) and after (solid) ultrasonic treatment. The NIR measurement was taken for the sands after ultrasonic treatment and being washed by deionized water.

When the coating mass decreased to 1.6 mg (~0.5 mg/cm^2), the characteristic bands of clay minerals could be still well-distinguished, but with very low intensities. The absorption band at *ca.* 2.16 μm of kaolinite became obscure to disappear for the coating mass below 8.0 mg.

The NIR spectra of the physically mixed basalt grains (Martian soil analogues) and clay minerals (Fig. 8) showed that the intensity of the characteristic bands of clay minerals decreased with the decrease of the proportions. When their contents were reduced to 5 $_{wt}$%, respectively, the band intensity became very low, but well-distinguished. Further reduction of the content to 1$_{wt}$% would generate a noisy spectrum, which the band depth at 2.20/2.32 μm decreased by more than 80%.

4. Discussion

4.1. Occurrence state of clay minerals

4.1.1. Clay coatings on light-colored samples

The detrital materials on the surface of light-colored grains (IL1, IL4, IIIL1 and IVL1) collected in Qaidam Basin were mainly composed of quartz, and small amounts of illite and chlorite, as indicated by both XRD and NIR results (Figs. 3 and 4). These clay minerals showed a foliated morphology in SEM images (Fig. 5), which was consistent with those generally observed in the weathered samples. For the sample IL1, EDS analyses indicated that the atom ratio of Si/Al was 1.20 (S1), close to that of illite, while the Fe content (S2) was higher than that of S1 (Figs. 5 and S4), implying the existence of chlorite (a Fe-rich clay mineral).

After ultrasonic treatment for 20 min, illite and chlorite were still present on the surface of sands as indicated by NIR spectra (Fig. 4). The deduction was supported by EDS tests of the selected spots, which showed the existence of silicon, iron and aluminum on the quartz surface (Figs. 5 and S4). Among them, S3 showed a Si/Al ratio of 1.72 (close to that of illite), and S4 showed the presence of Fe. The high Si/Al ratio as 14 from S5 suggested the precipitation of amorphous silica on the sands (Figs. 5 and S4). The EPMA data further indicated that there was a significant difference between the elemental composition of the surface and the interior substrate (Table 3; Figs. 6e-h). Fe and Al were preferentially enriched in the surface coatings, while little (or even no) Fe and Al in the interior substrate. Accordingly, it was proposed that clay minerals were physically adsorbed on the light-colored quartz as dust coating, and further masked by amorphous silica lately reprecipitated from the substrate rocks.

4.1.2. Clay coatings on dark-colored samples

Illite and chlorite could still exist on the surface of the field samples with black to brown coatings, after a 50-min ultrasonic treatment, as evidenced by XRD and NIR results (Figs. 3 and 4). BSE images of the rock thin sections showed that the coatings were distinct from the substrates in morphology (Figs. 6a-d). The related EPMA data indicated that the

Table 3
EPMA analyses of the thin sections of the samples ($_{wt}$%).

	Element	Na_2O	FeO	K_2O	SiO_2	MnO	Cl	Al_2O_3	Cr_2O_3	CaO	MgO	TiO_2	Total
IID1	P1	6.46	0.10	0.05	88.25	0.03	0.02	4.67	0.28	0.06	–	0.02	99.94
	P2	0.06	–	0.03	99.12	0.01	–	0.14	0.04	0.01	–	–	99.41
	P3	0.05	–	0.01	98.51	–	–	0.28	0.00	0.03	–	–	98.88
ID2	P1	3.31	0.47	5.76	86.74	0.03	0.00	2.77	0.02	0.05	–	0.17	99.32
	P2	0.25	0.09	9.75	89.22	–	–	0.36	0.00	0.01	–	–	99.68
	P3	0.02	0.06	–	98.81	0.00	0.00	0.05	–	0.00	0.01	0.04	99.00
ID3	P1	2.65	0.12	0.16	91.09	0.02	0.01	6.08	–	0.28	–	0.04	100.44
	P2	–	0.05	0.01	99.28	0.02	–	0.04	–	0.02	–	0.07	99.49
	P3	–	0.02	–	99.91	–	0.01	0.03	0.07	0.02	–	0.04	100.10
IL1	P1	0.20	0.07	1.95	95.63	–	0.00	1.56	0.00	–	0.00	0.10	99.52
	P2	0.12	0.00	–	98.85	–	–	0.05	–	–	–	–	99.02
	P3	0.00	0.00	–	99.26	–	0.00	0.01	–	–	–	0.02	99.29
IL4	P1	0.05	0.03	0.01	97.89	–	–	1.08	–	0.01	–	–	99.07
	P2	0.08	–	0.04	99.54	–	0.03	0.07	–	0.10	–	0.03	99.88
	P3	0.04	–	0.01	100.60	–	0.01	–	0.04	0.00	0.01	–	100.72
IIIL1	P1	0.06	0.02	0.03	99.12	–	–	0.14	0.04	0.01	–	–	99.42
	P2	0.05	–	0.06	99.51	–	–	0.00	0.00	0.03	–	–	99.65
	P3	–	–	–	99.91	–	–	–	0.01	0.01	–	0.01	99.94
IVL1	P1	0.01	0.03	0.08	99.07	–	0.01	0.24	–	–	0.00	0.03	99.46
	P2	0.07	0.00	0.03	98.92	–	0.00	–	0.00	0.02	0.00	0.05	99.11
	P3	0.01	–	0.01	99.41	–	0.01	–	0.02	–	–	0.01	99.47

Note. For the each samples, the first point (P1) was located in outer coatings and the other points (P2 and P3) were located in inner substrates.

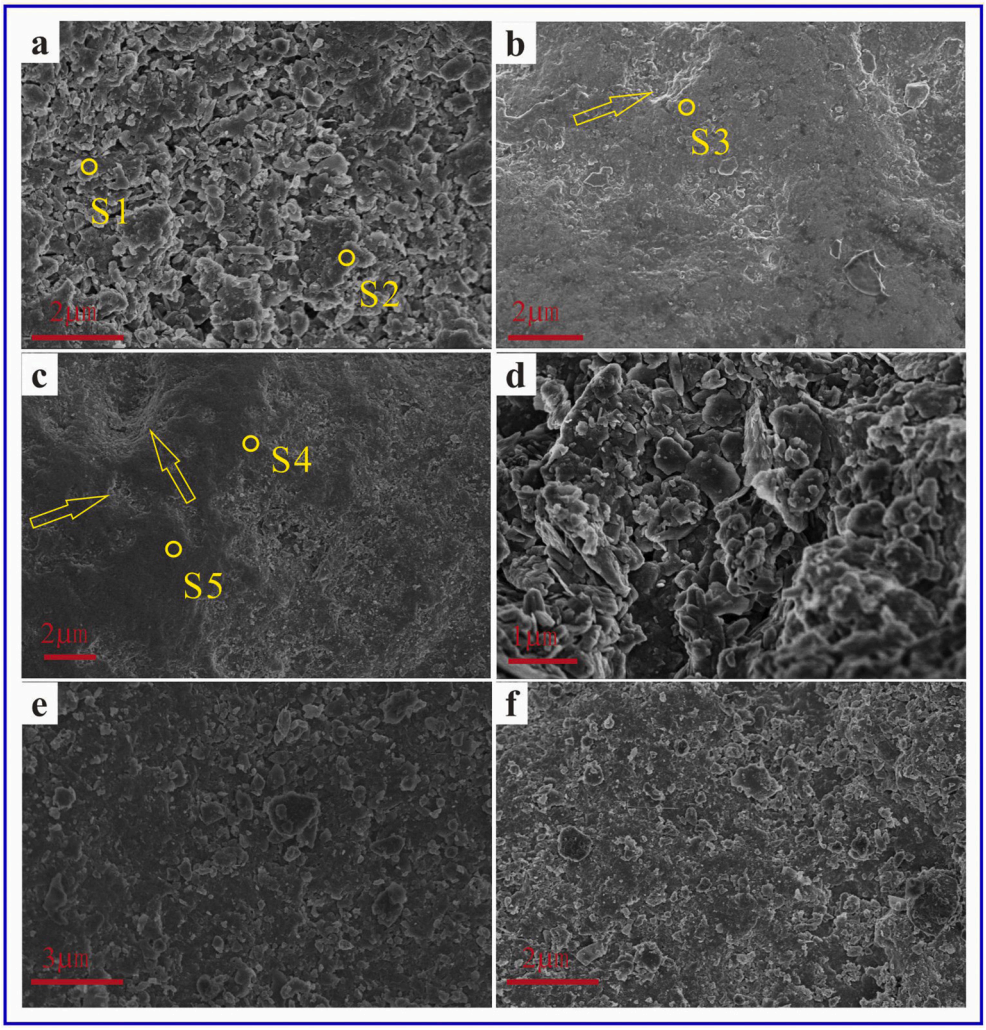

Fig. 5. SEM images of field samples. (a) IL1 (before ultrasonic treatment); (b) and (c) IL1 (after ultrasonic treatment); (d) IL4 (after ultrasonic treatment); (e) IIIL1 (before ultrasonic treatment); (f) IV1 (before ultrasonic treatment). The yellow arrows indicate the location of corrosion and impact pits in samples.

coatings were much richer in Fe, Mg, Al and Mn than that of the substrate (Table 2). The highest contents were up to 0.47% and 0.03% for Fe and Mn, respectively. Rock varnish is ubiquitous on the earth, and particularly abundant in arid and semiarid regions, such as desert and gobi (Goldsmith et al., 2014; Macholdt et al., 2015, 2017; Sarmast et al., 2017). Qaidam Basin has developed an extremely dry climate (Xiao et al., 2017), which is suitable for the generating of desert varnish. Based on the above results, it was concluded that the coatings on the surface of dark-colored sands in these cases belong to desert varnish masked by clay minerals and amorphous silica.

4.2. *Influences of coatings on the NIR detections*

The present Synthesized samples A-C indicated that even thin coatings of clay minerals are sufficient to mask the spectral signature of substrate during NIR tests, no matter the type of clay minerals. The clay coating, with a 0.21 $_{wt}$% content or with a thickness of ~2.1 μm (0.5 mg/cm^2), were enough to induce well-distinguished NIR bands as in Synthesized samples A (Table 1; Fig. 7a) and Synthesized samples B (Figs. 6 and 7b), respectively.

To further analyze the influences of different clay coatings on the NIR spectra, the band depth of their distinctive bands were calculated (Viviano-Beck et al., 2014; Liu et al., 2021; Du et al., 2020) as a function of the clay mineral contents in Synthesized samples A and B (Fig. 9). The values were then compared with those of the physically mixed samples (Martian soil analogues with 1-55 $_{wt}$% each clay minerals) as in Synthesized samples C (black spots in Fig. 9).

The band depth of the characteristic bands in NIR spectra of the four coatings in Synthesized samples A (red diamond) was equivalent to that of the Martian soil analogues (Meslin, 2013) with 12 to 24 $_{wt}$% clay mineral contents of as in Synthesized samples C. Meanwhile, for the clay coatings on polished quartz as in Synthesized samples B (blue triangle), the calculated band depth of the ones with thicknesses of 2.1 μm (0.5 mg/cm^2) were equivalent to that of the Martian soil analogues with 4 to 7 $_{wt}$% clay minerals as in Synthesized samples C.

The mass ratio of clay coating on the rock surface was highly related to the particle size of the substrate. The larger the rock size, the smaller the relative total specific surface area, and the smaller the mass ratio of the masked clay minerals accordingly. For the sands with particle size of 5 mm (belongs to fine gravel), the maximum mass ratio of clay coatings was only 0.51 $_{wt}$% as in Synthesized samples A. Gravels mainly with much higher sizes and rounded to sub-rounded appearances in morphology (e.g. pebbles and cobbles with a size of 4–64 mm and 64–256 mm, respectively), as widely distributed on the surface of Mars (Wentworth, 1922; Williams et al., 2013; Yingst et al., 2013; Szabó et al., 2015), should hold smaller mass ratio of clay coatings. However, the above Synthesized samples A-C showed that clay coatings, even with very a small mass ratio, could lead to well-distinguished NIR bands. Its band depth could reach the value of Martian soil with much higher clay content (4-24 $_{wt}$%). Therefore, it was reasonably proposed that the clay

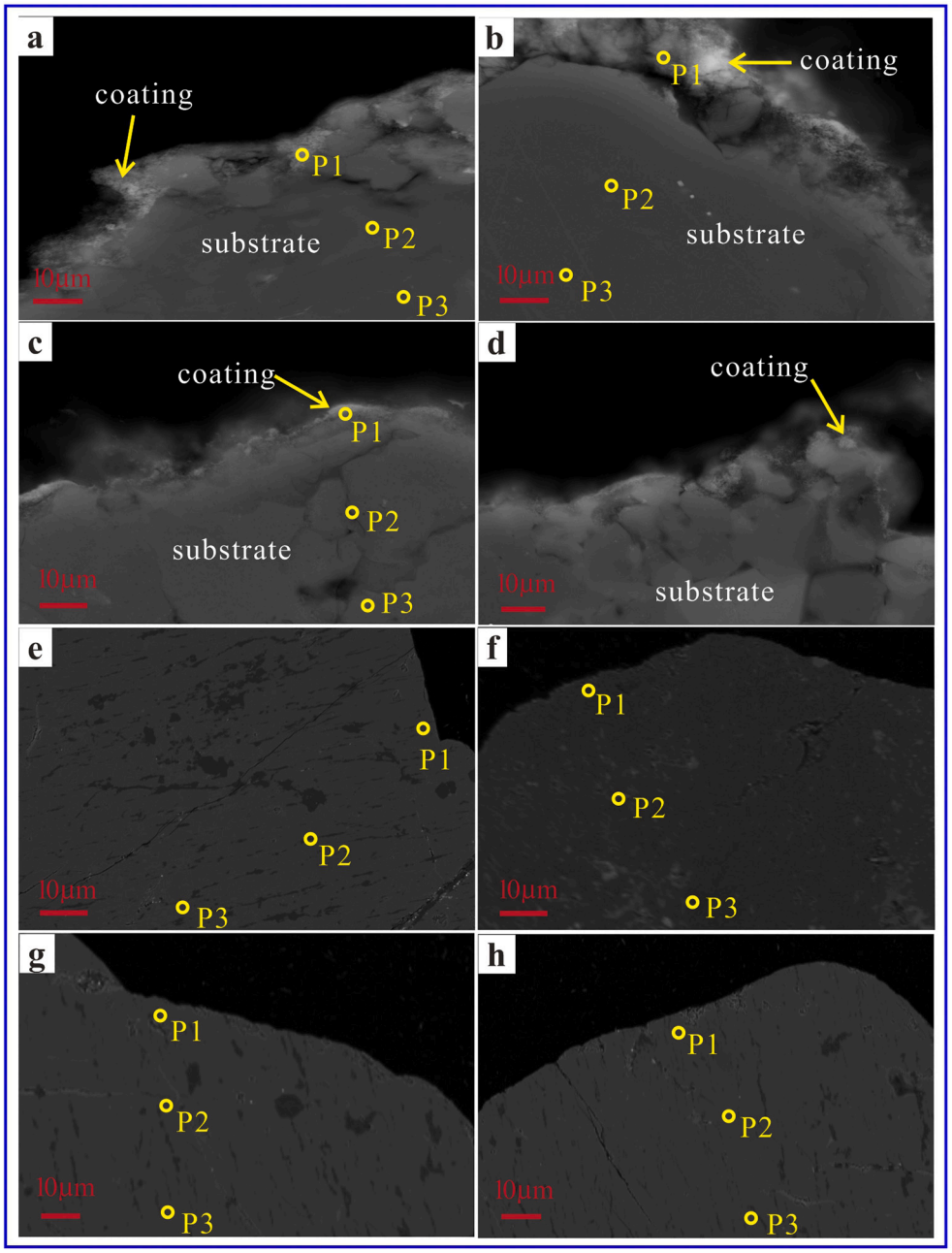

Fig. 6. Back scattered electron (BSE) images of rock thin section of samples. (a) ID2; (b) ID3; (c,d) IID1; (e) IL1; (f) IL4; (g) IIIL1; (h) IVL1. The yellow points was the location of EPMA.

coating might affect the content, distribution and occurrence determination of clay minerals on the surface of Mars by remote sensing.

4.3. Origin of clay minerals in Qaidam Basin

The above analyses showed the evidence that quartz was the leading component mineral in the substrate rocks in Qaidam Basin, while clay minerals were distributed on the surface as coatings. There are generally two kinds of coated clay mineral origins in an arid desert environment, *i.e.*, authigenic and aeolian origins. They can be distinguished by the morphology of the contained clay minerals. Taking assemblage of illite and chlorite as an example, the aeolian ones usually show irregular clastic in morphology, which is coincided with those in this cases as shown in Fig. 5 (Maxime et al., 2019). While authigenic illite and chlorite usually display regular foliated, rose-shaped morphology (Tompkins, 1981). One the other hand, literatures showed that there are some relations with the geologic context. In marginal marine systems, continental shelf and slope, and basin plain sediments, the origin of clay coatings was probably related to adhesive biofilms (Dowey et al., 2012; Wooldridge et al., 2017). In the context of Gobi and desert, it is favorable for the formation of clay coatings in form of desert varnish and silica coatings (i.e. silica glaze, a hydrated silica (opal) that accretes on the surfaces of sands in all deserts) (Smoot, 1995). It is generally believed that desert varnish is aeolian deposit (Dorn, 2009; Fox et al., 2016). According to the chemistry, if the clay coatings were authigenic, the compositions of the coatings should be similar to that of the substrates. However, the chemical composition of the substrates was quite different from that of the coatings by EPMA analysis (Fig. S3, Table 3). For authigenic clay minerals, water is an essential condition for their formation (Ehlmann et al., 2009; He et al., 2013). The climate of Qaidam

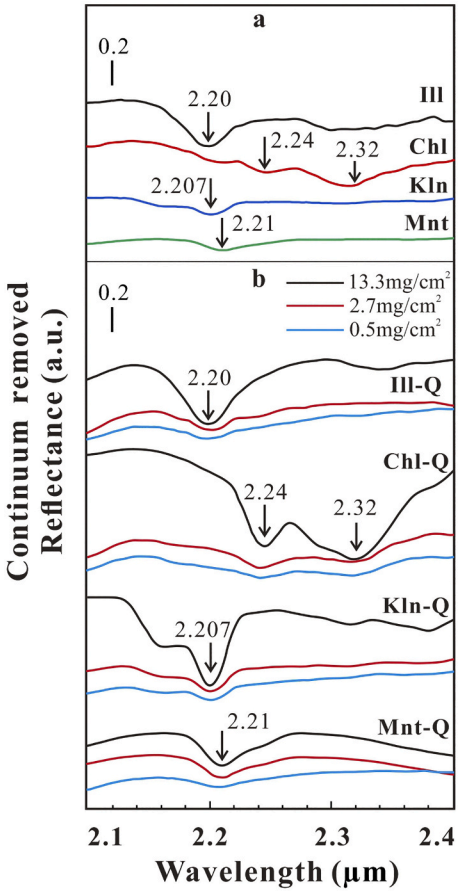

Fig. 7. (a) NIR reflectance spectra of the samples in Synthesized samples A; (b) NIR reflectance spectra of coating analogues with four clay minerals on the polished quartz in Synthesized samples B.

Basin is extremely dry and authigenic clay minerals are unlike to form. Previous studies indicated that the minerals on substrates could be a global weathering product on Mars (Bishop et al., 2002). However, the weathering on Earth is stronger than that on Mars (Perry and Sephton, 2006), leading to clay minerals with weaker weathering resistance (such as illite and chlorite coatings in this paper) can only be transported for a short distance. Based upon the above discussions, we conclude that the illite and chlorite coating in the used samples are with an aeolian origin. They might originate from the deposits/shale in the deep crust, and then were uplifted by tectonic movement and transported by wind after physical weathering, which was supported by the data of the core log in Charhan playa and the illite and chlorite outcrop and soil on the Qilian Mountain in the north of Qaidam Basin (Zhang et al., 1997; He, 2020). Recent studies have shown that clay coatings based on sandstone (the main mineral is quartz) may be viewed as a biosignature (Wooldridge et al., 2017; Duteil et al., 2020). However, we did not find any substance related to microbes (e.g. biofilms) by SEM in this case.

The surface sediments of the sampling sites are mainly composed of quartz, which usually had strong weathering resistance. Their excellent roundness indicated that they had experienced strong erosions by wind (Fig. 2) (Zhao et al., 2017; Hossain et al., 2020). The Kunlun Mountains in the southern margin of Qaidam Basin were dominated by metamorphic rocks, acidic magmatic rocks and a small amount of carbonate rocks. Therefore, the quartz grains in the sampling regions were proposed to have been transported from the surrounding weathered mountain areas (Liu et al., 2013; Bao and Dong, 2015).

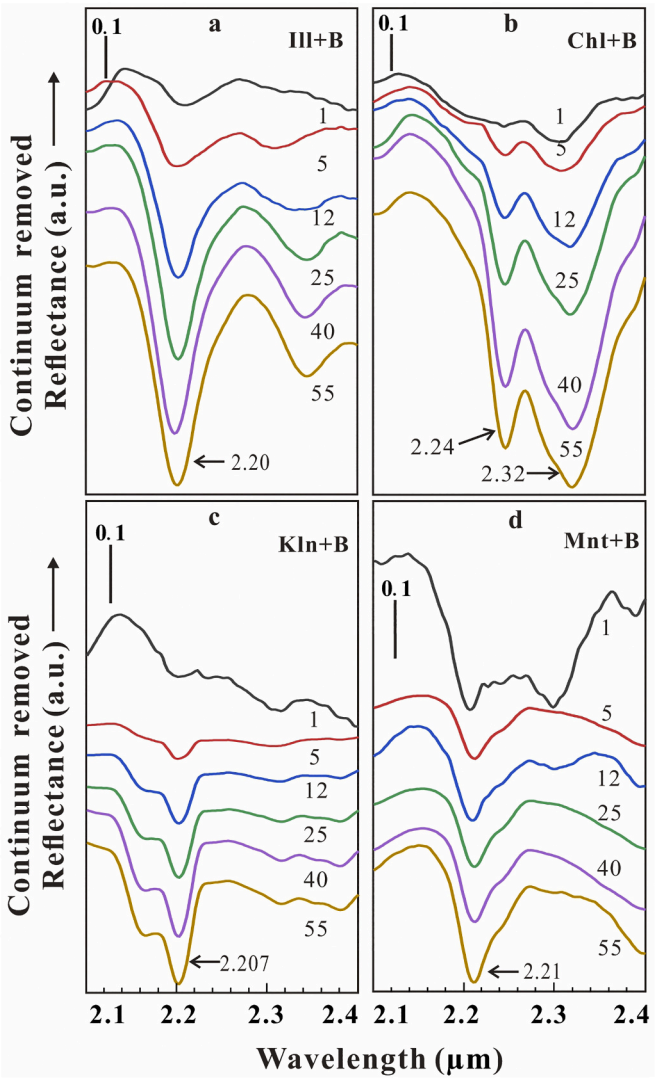

Fig. 8. NIR reflectance spectra of samples in Synthesized samples C. The numbers of 1, 5, 12, 25, 40 and 55 are the mass ratio of clay minerals ($_{wt}$%).

4.4. Implications on Mars

4.4.1. Distribution and occurrence state of clay minerals

Rock coatings are ubiquitous on Earth, but the study related to clay coatings as collected in the Qaidam Basin was rarely reported. Our study shows that various types of rock coatings (e.g., dust coating, silica coating and desert varnish) with tiny amounts of clay minerals may occur in the western Qaidam Basin. The Basin with an extremely arid and cold climate has been considered as a unique analogue to Mars (Xiao et al., 2017). Environmental similarities between western Qaidam Basin and Martian surface suggest that various clay coatings potentially exist on Mars and could affect the detection of minerals by remote sensing.

Evidences on the paleosurfaces and geological events of Mars suggest that physical and chemical weathering was less aggressive than that on Earth, and therefore various kinds of coatings could be better preserved (Morris and Rodionov, 2006; Perry and Sephton, 2006; Northup et al., 2010; Ody et al., 2012). About a third of the Earth's land had been experienced a semi-arid, arid, hyperarid climate (Abrahams and Parsons, 2009), which is favorable for the occurrence of desert varnish and silica coatings (i.e., silica glaze, a hydrated silica (opal) that accretes on the surfaces of sands in all deserts) (Smoot, 1995). Considering that Mars was more arid than Earth, it could be reasonably proposed that at least 30% of the surface of Mars was conducive to the formation of various

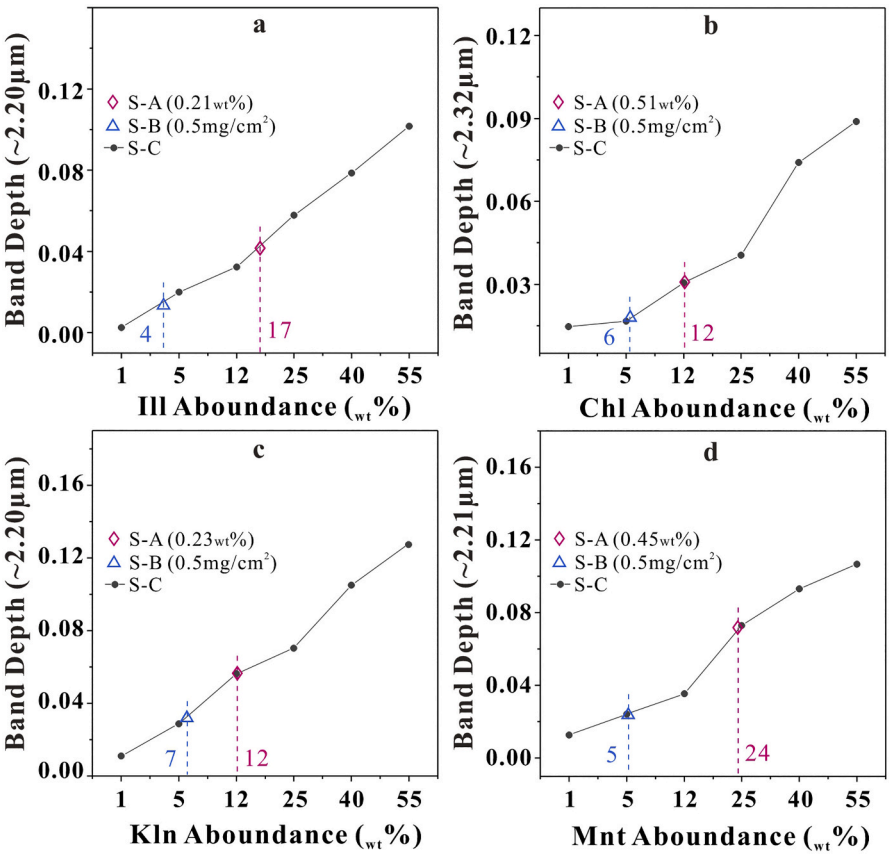

Fig. 9. Band depth of main bands. (a) Illite and basalt; (b) Chlorite and basalt. (c) Kaolinite and basalt; (d) Montmorillonite and basalt. Pink diamonds indicate the band depth in Synthesized samples A. Blue triangles indicate the band depth in Synthesized samples B (0.5 mg/cm2). The numbers highlighted next to the dashed lines were the band depth value that Synthesized samples A and Synthesized samples B corresponded to Synthesized samples C. S-A, Synthesized samples A; S-—B, Synthesized samples B; S-—C, Synthesized samples C.

kinds of clay coatings.

Clay minerals, mainly Fe/Mg smectite and chlorite, have already been found in coexistence with opaline silica, such as in Noachian terrain west of Nili Fossae, many of which are around impact craters (Ehlmann et al., 2009). Meanwhile, the silica deposits (i.e., hydrated silica) had been suggested as regionally or globally occurring phenomena on the Martian surface (Chemtob et al., 2010; Sun and Milliken, 2018). Moreover, the arid and semi-arid climate is most conducive to the formation of the clay coatings depending on silica as substrate (e.g., silica glaze and desert varnish) (Smoot, 1995; Abrahams and Parsons, 2009). The opaline silica could be dissolved and precipitated to form amorphous silicate during arid climate, which has similar chemical composition but relatively larger surface area than that of quartz. Therefore, it could be reasonably proposed that there were clay coatings which exist on silica substrate on the surface of the Mars (Ehlmann et al., 2009; Ehlmann and Edwards, 2014). However, the clay coatings formed in this way could have less effect due to small amount of outcrop of opaline silica on Mars (Ehlmann and Edwards, 2014). The greatest effect of clay coatings on remote sensing detection using near-infrared spectroscopy was probably resulted by the basaltic sands on Mars. Although the detrital grains distributed on the surface of Mars are dominated by basaltic sands instead of quartz, clay coatings (i.e. desert varnish) can also develop on basaltic materials to influence the remote sensing (Palmer, 2002). The content of clay minerals cemented in desert varnish could be up to 2/3 (Dorn, 1998). Desert varnish is a thin layer in black, red or brown and independent of the underlying substrate, which is widely distributed in arid and semi-arid environments (Abrahams and Parsons, 2009). It is generally believed that rock varnish is aeolian deposit (Dorn, 2009; Fox et al., 2016). Therefore, if the basalt sands with desert varnish were detected on the surface of Mars, the clay minerals in desert varnish may also be adsorbed, originating from underground deposits due to the excavation and dissemination by meteorite impacts, which were eventually captured during coatings formation. This proposition is consistent with the occurrence and origin of clay coatings from the Qaidam Basin. In addition, authigenic clay coatings had also been found on Hawaiian basalts (Meunier et al., 2008). If basaltic sands with clay coatings were detected on the surface of Mars, it could be related to hydrothermal alteration or degassing of lavas (Chevrier et al., 2007; Meunier et al., 2008).

Most importantly, our laboratory Synthesized samples A-C indicated that clay coatings, even with a very small mass ratio, could lead to well-distinguished NIR bands, whose band depth could reach the value of Martian soil with much higher clay content (Bridges et al., 2015). Therefore, they may affect the detection of the distribution and occurrence state of the local or globally clay minerals. Smectites in Endeavour Crater only shows a weak NIR band by CRISM, which is potentially caused by such a varnish analogue (Fox et al., 2016). About one third of the Earth's land is in arid climate. This hints that there is probably not as much clay minerals on the surface of Mars as previously proposed (such as in Northern lowlands) (Ehlmann and Edwards, 2014).

The present study suggests that the characteristics and distribution of various kinds of coatings should be fully considered in the determination of abundance and occurrence state of clay minerals on the global scale of Mars, along with the related paleogeography and geological events.

4.4.2. *Influence for mineral identification*

During the remote sensing detection on Mars, the site (e.g., sand dune that was considered to have the least interference) near the target was usually selected as the reference for ratio processing to abate noise (Thomson et al., 2011). Therefore, the selection of reference was important for the accuracy of mineral identification. In our laboratory Synthesized samples A-C, the ratioed reflectance of Martian soil analogues with 12_{wt} % or 25_{wt} % clay minerals as in Synthesized samples C was obtained by taking the related clay coating as in Synthesized samples A as the reference (Fig. 10). The results indicated that the distinctive clay bands of Martian soil analogues with 12 $_{wt}$% or 25 $_{wt}$% clay

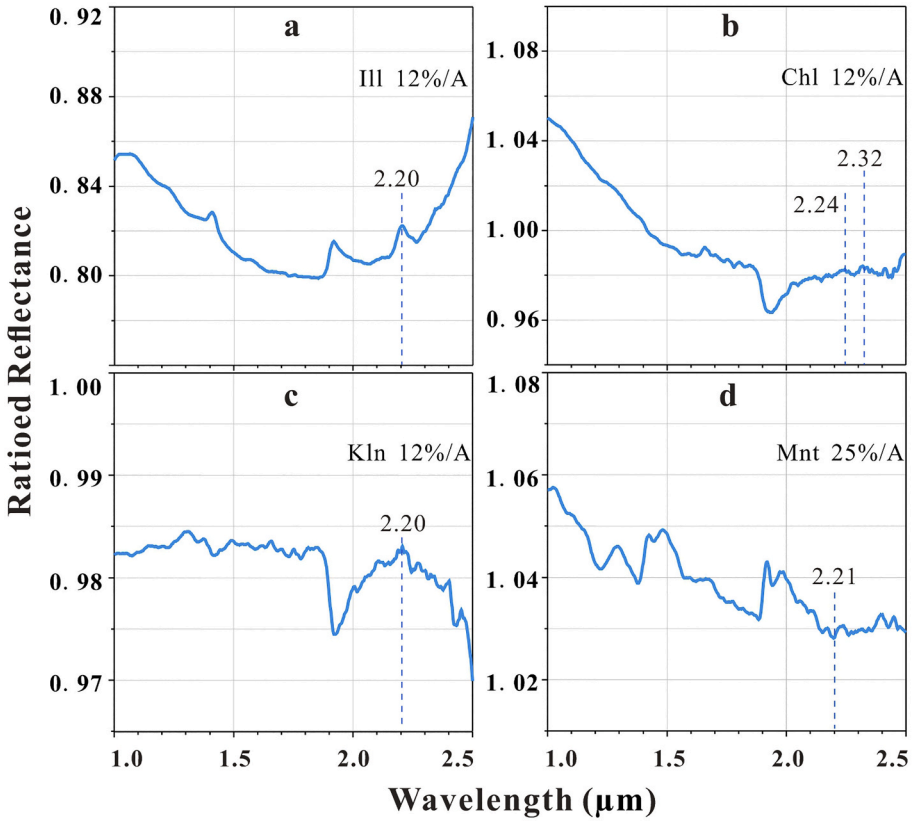

Fig. 10. Ratioed reflectance with the clay coating reflectance in Synthesized samples A as reference and the Martian soil analogues with 12_{wt}% or 25_{wt}% clay minerals in Synthesized sample C as detection coverage. (a) Illite; (b) Chlorite; (c) Kaolinite; (d) Montmorillonite.

minerals were instead weakened or abated when the sand dune with clay coating was chosen as the reference. In Gale crater on Mars, many sites did not detect clay minerals by remote sensing (Fraeman et al., 2016), but about 20 $_{wt}$% clay minerals that occurred in mudstones were deduced by XRD from the Mars Science Laboratory rover Curiosity (Bristow et al., 2018). These detections by remote sensing could have been influenced by the sand dune with clay coatings as the reference. Our analyses indicated that, if sand dunes with clay coatings were selected as the reference for ratio processing, the obtained clay reflectance could be weakened or abated during remote sensing detection to interfere the mineral identification.

5. Conclusions

The detrital sands containing clay coatings (dust coatings, silica coatings and desert varnish) were collected in the western Qaidam Basin. The elemental and phase compositions of the coatings and substrates were analyzed by a combination of techniques (e.g., NIR, XRD, EPMA, SEM). The results showed that the main phases of the coatings and substrates are illite and chlorite, and quartz, respectively. The color differences of detrital sands in morphology are mainly resulted from the distribution variations of the chromogenic metal cations (e.g., Fe and Mn) on the surface and in the interior of the quartz. The mineralogical analysis further indicated that the origin of clay minerals was aeolian in Qaidam Basin, and they were transported from close source area and captured during coating formation. Synthesized samples experiments showed that, apart from the influence of color, the NIR absorption intensity of the samples was mainly determined by the coating composition and the occurrence state of the coating on the substrate. Analogues samples, from both the field and Martian soil, indicated that clay coatings, even with several micrometers in thickness and/or trace amount (~0.5 mg/cm^2) could lead to well-distinguished NIR bands, and reach a large band depth as those measured from Martian soil analogues with ~5 $_{wt}$% to 25_{wt}% clay minerals at 2.20–2.40 μm. Considering the environmental similarities between western Qaidam Basin and Martian surface, it was further proposed that various rock coatings were also widespread on Mars. Therefore, the detection of clay minerals on the Martian surface could be consequently influenced. It is necessary to fully and thoroughly consider the distribution and characteristics of various coatings during the determination of abundance and occurrence state of clay minerals on the global scale of Mars. Moreover, our analyses about ratioed reflectance indicated that clay coatings could also influence the accuracy of mineral identification by remote sensing.

Author statement

Yonglei Zhang designed the experiments, analyzed the data and wrote the manuscript.

Qi Tao was involved in conception proposal, funding acquisition, manuscript discussion and revision.

Sridhar Komarneni was involved in the revision of the manuscript.

Jiacheng Liu was involved in the discussion.

Yang Zhou was involved in the discussion of the manuscript.

Fan Yang was involved in the revision of the manuscript.

Baifa Zhang was involved in the characterization of the samples.

Declaration of Competing Interest

The authors declare that there is no conflict of interest.

Acknowledgments

This research was jointly supported by National Natural Science Foundation of China (Grant numbers 42072044, 41921003) and Science

and Technology Plan of Guangdong Province (2020B1212060055).

Appendix A. Supplementary data

Supplementary data to this article can be found online at https://doi.org/10.1016/j.clay.2021.106065.

References

Abrahams, A., Parsons, A., 2009. Geomorphology of Desert Environments. Springer, Dordrecht, pp. 3–7.

Bao, F., Dong, Z., 2015. Mineral composition and origin of surface sediment in the desert of Qaidam Basin. J. Northwest Uni. 45 (1), 90–96.

Bibring, J., Langevin, Y., Mustard, J., Poulet, F., Arvidson, R., Gendrin, A., Neukum, G., 2006. Global mineralogical and aqueous Mars history derived from OMEGA/Mars express data. Science 312, 400–404.

Bishop, J., Murchie, S., Pieters, C., Zent, A., 2002. A model for formation of dust, soil, and rock coatings on Mars: physical and chemical processes on the Martian surface. J. Geophys. Res. 265, 69–84.

Bishop, J., Lane, M., Dyar, M., Brown, A., 2008. Reflectance and emission spectroscopy study of four groups of phyllosilicates: smectites, kaolinite-serpentines, chlorites and micas. Clay Miner. 43, 35–54.

Bridges, J., Schwenzer, S., Leveille, R., Westall, F., Wiens, R., Mangold, N., Berger, G., 2015. Diagenesis and clay mineral formation at Gale Crater, Mars. J. Geophys. Res. 120 (1), 1–19.

Bristow, T., Rampe, E., Achilles, C., Blake, D., Chipera, S., Craig, P., Grotzinger, J., 2018. Clay mineral diversity and abundance in sedimentary rocks of Gale crater, Mars. Sci Adv. 4 (6) eaar3330.

Carter, J., Poulet, F., Bibring, J., Murchie, S., 2010. Detection of hydrated silicates in crustal outcrops in the northern plains of Mars. Science 328, 1682–1686.

Chemtob, S., Jolliff, B., Rossman, G., Eiler, J., Arvidson, R., 2010. Silica coatings in the Ka'u Desert, Hawaii, a Mars analog terrain: a micromorphological, spectral, chemical, and isotopic study. J. Geophys. Res. 115 (E04001).

Chemtob, S., Nickerson, R., Morris, R., Agresti, D., Catalano, J., 2015. Synthesis and structural characterization of ferrous trioctahedral smectites: implications for clay mineral genesis and detectability on Mars. J. Geophys. Res. 120, 1119–1140.

Chen, K., Bowler, J., 1986. Late Pleistocene evolution of salt lakes in the Qaidam basin, Qinghai province, China. Palaeogeogr. Palaeocl. 54, 87–104.

Chen, B., Wang, F., Shi, J., Chen, F., Shi, H., 2019. Origin and sources of minerals and their impact on the hydrocarbon reservoir quality of the paleogenelulehe formation in the Eboliang Area, Northern Qaidam Basin, China. Minerals 9, 436.

Chevrier, V., Poulet, F., Bibring, J., 2007. Early geochemical environment of mars as determined from thermodynamics of phyllosilicates. Nature 448, 60–63.

Christensen, P., 2004. Initial results from the Mini-TES experiment in Gusev Crater from the Spirit Rover. Science 305, 837–841.

Cino, C., Dehouck, E., McLennan, S., 2017. Geochemical constraints on the presence of clay minerals in the Burns formation, Meridiani Planum, Mars. Icarus 281, 137–150.

Clark, R., Roush, T., 1984. Reflectance spectroscopy: quantitative analysis techniques for remote sensing applications. J. Geophys. Res. Solid Earth 89, 6329–6340.

Clark, B., Morris, R., Herkenhoff, K., Farrand, W., Gellert, R., Jolliff, B., Yen, A., 2016. Esperance: Multiple episodes of aqueous alteration involving fracture fills and coatings at Matijevic Hill, Mars. Am. Mineral. 101 (7), 1515–1526.

Cuadros, J., Michalski, J., Dekov, V., Bishop, J., Fiore, S., Dyar, M., 2013. Crystal-chemistry of interstratified Mg/Fe-clay minerals from seafloor hydrothermal sites. Chem. Geol. 360, 142–158.

Dang, Y., Xiao, L., Xu, Y., Zhang, F., Huang, J., Wang, J., Yue, Z., 2018. The polygonal surface structures in the Dalangtan Playa, Qaidam Basin, NW China: controlling factors for their formation and implications for analogous Martian landforms. J. Geophys. Res. 123, 1910–1933.

Dorn, R., 1998. Rock coatings. In: Elsevier; Developments in Earth Surface Processes, pp. 1–297.

Dorn, R., 2009. Desert Rock Coatings. In: Parsons, A.J., Abrahams, A.D. (Eds.), Geomorphology of Desert Environments. Springer, Dordrecht, pp. 153–186.

Dowey, P., Hodgson, D., Worden, R., 2012. Pre-requisites, processes, and prediction of chlorite grain coatings in petroleum reservoirs: a review of subsurface examples. Mar. Pet. Geol. 32, 63–75.

Du, P., Yuan, P., Liu, J., Yang, Y., Bu, H., Wang, S., Zhou, J., Song, H., 2020. Effects of environmental Fe concentrations on formation and evolution of allophane in Al-Si-Fe systems: implications for both Earth and Mars. J. Geophys. Res. 125.

Duteil, T., Bourillot, R., Grégoire, B., Virolle, M., Brigaud, B., Nouet, J., Gontier, E., 2020. Experimental formation of clay-coated sand grains using diatom biofilm exopolymers. Geology 48 (10), 1012–1017.

Ehlmann, B., Edwards, C., 2014. Mineralogy of the Martian surface. Annu. Rev. Earth. Pl. Sc. 42, 291–315.

Ehlmann, B., Mustard, J., Swayze, G., Clark, R., Bishop, J., Poulet, F., Barnouin-Jha, O., 2009. Identification of hydrated silicate minerals on Mars using MRO-CRISM: Geologic context near Nili Fossae and implications for aqueous alteration. J. Geophys. Res. 114 (10).

Ehlmann, B., Berger, G., Mangold, N., Michalski, J., Catling, D., Ruff, S., Poulet, F., 2013. Geochemical consequences of widespread clay mineral formation in Mars' ancient crust. Space Sci. Rev. 174, 329–364.

Farrand, W., Johnson, J., Rice, M., Wang, A., Bell, J., 2016. VNIR multispectral observations of aqueous alteration materials by the Pancams on the Spirit and Opportunity Mars Exploration Rovers. Am. Mineral. 101 (9), 2005–2019.

Fox, V., Arvidson, R., Guinness, E., Mclennan, S., Catalano, J., Murchie, S., 2016. Smectite deposits in Marathon valley, Endeavour crater, Mars, identified using crism hyperspectral reflectance data. Geophys. Res. Lett. 43 (10), 4885–4892.

Fraeman, A., Ehlmann, B., Arvidson, R., Edwards, C., Grotzinger, J., Milliken, R., Rice, M., 2016. The stratigraphy and evolution of lower Mount Sharp from spectral, morphological, and thermophysical orbital data sets. J. Geophys. Res. 121 (9), 1713–1736.

Gaudin, A., Dehouck, E., Grauby, O., Mangold, N., 2018. Formation of clay minerals on Mars: insights from long-term experimental weathering of olivine. Icarus 311, 210–223.

Goldsmith, Y., Stein, M., Enzel, Y., 2014. From dust to varnish: Geochemical constraints on rock varnish formation in the Negev Desert, Israel. Geochim. Cosmochim. Acta 126, 97–111.

Guan, J., Liu, A., Xie, K., Shi, Z., Kubikova, B., 2020. Preparation and characterization of Martian soil simulant NEU Mars-1. T Nonferr Metal Soc. 30, 212–222.

Hamilton, V., Christensen, P., 2005. Evidence for extensive, olivine-rich bedrock on Mars. Geology 33, 433–436.

He, Y., 2020. Soil Genetic Characteristics and Taxonomic Classification of Beishan Forest Region in Qilian Mountains. Beijing Forestry University, Beijing (in Chinese).

He, H., Tao, Q., Zhu, J., Yuan, P., Shen, W., Yang, S., 2013. Silylation of clay mineral surfaces. Appl. Clay Sci. 71, 15–20.

Hossain, H., Armstrong-Altrin, J., Jamil, A., Rahman, M., Hernández-Coronado, C., Ramos-Vázquez, M., 2020. Microtextures on quartz grains in the Kuakata beach, Bangladesh: implications for provenance and depositional environment. Arab. J. Geosci. 13 (7), 1–12.

Kraft, M., Michalski, J., Sharp, T., 2003. Effects of pure silica coatings on thermal emission spectra of basaltic rocks: considerations for Martian surface mineralogy. Geophys. Res. Lett. 30 (24).

Lefebvre, C., Catala-Espi, A., Sobron, P., Koujelev, A., Leveille, R., 2016. Depth-resolved chemical mapping of rock coatings using laser-induced breakdown spectroscopy: implications for geochemical investigations on Mars. Planet Space Sci. 126, 24–33.

Liu, T., Broecker, W., Stein, M., 2013. Rock varnish evidence for a Younger Dryas wet period in the Dead Sea basin. Geophys. Res. Lett. 40, 2229–2235.

Liu, J., He, H., Michalski, J., Cuadros, J., Yao, Y., Tan, W., Qin, X., Li, S., Wei, G., 2021. Reflectance spectroscopy applied to clay mineralogy and alteration intensity of a thick basaltic weathering sequence in Hainan Island, South China. Appl. Clay Sci. 201.

Macholdt, D., Jochum, K., Pöhlker, C., Stoll, B., Weis, U., Weber, B., Weigand, M., 2015. Microanalytical methods for in-situ high-resolution analysis of rock varnish at the micrometer to nanometer scale. Chem. Geol. 411, 57–68.

Macholdt, D., Jochum, K., Pöhlker, C., Arangio, A., Förster, J., Stoll, B., Shiraiwa, M., 2017. Characterization and differentiation of rock varnish types from different environments by microanalytical techniques. Chem. Geol. 459, 91–118.

Marnocha, C., 2017. Rock coatings and the potential for life on Mars. Elements 13 (3), 187–191.

Marnocha, C., Dixon, J., 2013. Bacterial communities in Fe/Mn films, sulphate crusts, and aluminium glazes from Swedish Lapland: implications for astrobiology on Mars. Int. J. Astrobiol. 12, 345–356.

Maxime, V., Benjamin, B., Rapha, L., Féniès Hugues, E., Thibault, D., 2019. Detrital clay grain coats in estuarine clastic deposits: origin and spatial distribution within a modern sedimentary system, the gironde estuary (South-West France). Sedimentology 66, 859–894.

Meslin, P., 2013. Soil diversity and hydration as observed by ChemCam at Gale Crater, Mars. Science 341 (6153).

Meunier, A., Mas, A., Beaufort, D., Patrier, P., Dudoignon, P., 2008. Clay minerals in basalt-hawaiite rocks from mururoa atoll (French Polynesia). ii. Petrography and geochemistry. Clay Clay Miner. 56, 711–729.

Michalski, J., Fergason, R., 2009. Composition and thermal inertia of the Mawrth Vallis region of Mars from TES and THEMIS data. Icarus 199, 25–48.

Milliken, R., Swayze, G., Arvidson, R., Bishop, J., Clark, R., Ehlmann, B., Weitz, C., 2008. Opaline silica in young deposits on Mars. Geology 36, 847–850.

Minitti, M., Weitz, C., Lane, M., Bishop, J., 2007. Morphology, chemistry, and spectral properties of Hawaiian rock coatings and implications for Mars. J. Geophys. Res. 112 (E5).

Montagnac, G., Hao, J., Pedreira-Segade, U., Daniel, I., 2020. Detection of nucleotides adsorbed onto clay by UV resonant raman spectroscopy: a step towards the search for biosignatures on Mars. Appl. Clay Sci. 200, 105824.

Morris, R., Rodionov, D., 2006. Mo-ssbauer mineralogy of rock, soil, and dust at Meridiani Planum, Mars: opportunity's journey across sulfate-rich outcrop, basaltic sand and dust, and hematite lag deposits. J. Geophys. Res. 111 (E12).

Northup, D., Snider, J., Spilde, M., Porter, M., Bargar, J., 2010. Diversity of rock varnish bacterial communities from black canyon, new, Mexico. J. Geophys. Res.-Atmos. 115 (G2), 1–19.

Ody, A., Poulet, F., Langevin, Y., Bibring, J.P., Bellucci, G., Altieri, F., Manaud, N., 2012. Global maps of anhydrous minerals at the surface of Mars from OMEGA/MEx. J. Geophys. Res. 117 (E11).

Palmer, E., 2002. Feasibility and Implications of a Rock Coating Catena: Analysis of a Desert Hillslope. M.A. Thesis. Department of Geography, Arizona State University, Tempe.

Perry, R., Sephton, M., 2006. Desert varnish: an environmental recorder for Mars. Astron. Geophys. 47, 4–34.

Sarmast, M., Farpoor, M., Boroujeni, I., 2017. Soil and desert varnish development as indicators of landform evolution in central Iranian deserts. Catena 149, 98–109.

Schindler, M., Dorn, R., 2017. Coatings on rocks and minerals: the interface between the lithosphere and the biosphere, hydrosphere, and atmosphere. Elements 13 (3), 155–158.
Schubel, K., Lowenstein, T., 1997. Criteria for the recognition of shallow-perennial-saline-lake halites based on recent sediments from the Qaidam Basin, Western China. J. Paleolimnol. 44 (2), 431–442.
Seelos, K., Arvidson, R., Jolliff, B., Chemtob, S., Morris, R., 2010. Silica in a Mars analog environment: ka'u Desert, Kilauea Volcano, Hawaii. J. Geophys. Res. 115 (E4).
Smoot, N., 1995. Mass wasting and subaerial weathering in guyot formation: the Hawaiian and Canary Ridges as examples. Geomorphology 14, 29–41.
Stokes, R., 1945. Isopiestic vapor pressure measurements on concentrated solutions of sodium hydroxide at 25°C. J. Am. Chem. Soc. 67, 1689–1691.
Sun, V., Milliken, R., 2018. Distinct geologic settings of Opal-A and more crystalline hydrated silica on Mars. Geophys. Res. Lett. 45 (19), 10–221.
Szabó, T., Domokos, G., Grotzinger, J., Jerolmack, D., 2015. Reconstructing the transport history of pebbles on Mars. Nat. Commun. 6 (1), 1–7.
Thomson, B., Bridges, N., Milliken, R., Baldridge, A., Hook, S., Crowley, J., Weitz, C., 2011. Constraints on the origin and evolution of the layered mound in Gale Crater, Mars using Mars Reconnaissance Orbiter data. Icarus 214 (2), 413–432.
Tompkins, R., 1981. Scanning electron microscopy of a regular chlorite/smectite (corrensite) from a hydrocarbon reservoir sandstone. Clay Clay Miner. 29, 233–235.
Viviano-Beck, C., Seelos, F., Murchie, S., Kahn, E., Seelos, K., Taylor, H., Morgan, M., 2014. Revised CRISM spectral parameters and summary products based on the currently detected mineral diversity on Mars. J. Geophys. Res. 119 (6), 1403–1431.
Wentworth, C., 1922. A scale of grade and class terms for clastic sediments. J. Geol. 30, 377–392.
Williams, R., Grotzinger, J., Dietrich, W., Gupta, S., Sumner, D., Wiens, R., Forni, O., 2013. Martian fluvial conglomerates at Gale crater. Science 340 (6136), 1068–1072.
Wooldridge, L., Worden, R., Griffiths, J., Thompson, A., Chung, P., 2017. Biofilm origin of clay-coated sand grains. Geology 45 (10).
Wu, L., Xiao, A., Yang, S., Wang, L., Mao, L., 2012. Two-stage evolution of the Altyn Tagh Fault during the Cenozoic: new insight from provenance analysis of a geological section in NW Qaidam Basin, NW China. Terra Nova 24, 387–395.
Xiao, L., Wang, J., Dang, Y., Cheng, Z., Huang, T., Zhao, J., Komatsu, G., 2017. A new terrestrial analogue site for Mars research: the Qaidam Basin, Tibetan Plateau (NW China). Earth-Sci. Rev. 164, 84–101.
Xie, L., Pei, Y., Li, A., Wu, K., 2018. Implications of meso- to micro-scale deformation for fault sealing capacity: insights from the lenghu fold-and-thrust belt, Qaidam Basin, Tibetan Plateau. J. Asian Earth Sci. 158, 336–351.
Yingst, R., Kah, L., Palucis, M., Williams, R., Garvin, J., Bridges, J., Goetz, W., 2013. Characteristics of pebble- and cobble- sized clasts along the Curiosity rover traverse from Bradbury Landing to Rocknest. J. Geophys. Res. 118 (11), 2361–2380.
Yu, L., Lai, Z., 2012. OSL chronology and palaeoclimatic implications of aeolian sediments in the eastern Qaidam Basin of the northeastern Qinghai-Tibetan Plateau. Palaeogeogr. Palaeocl. 337, 120–129.
Zhang, R., Zhao, J., Shen, S., 1997. Early Paleozoic Marine Volcanic Sedimentary Facies and Geological Prospecting in the North Qilian Mountains. Geological Publishing House, Beijing. ISBN:7-116-02379-8 (in Chinese).
Zhao, X., Liu, Y., Salem, A., Marks, L., Welc, F., Sun, Q., Chen, Z., 2017. Migration of the Intertropical Convergence Zone in North Africa during the Holocene: evidence from variations in quartz grain roundness in the lower Nile valley, Egypt. Quat. Int. 449, 22–28.